Atomic force microscopy of gastric mucin and chitosan mucoadhesive systems

Matthew P. DEACON*†, Simon McGURK†, Clive J. ROBERTS†, Phillip M. WILLIAMS†, Saul J. B. TENDLER†, Martyn C. DAVIES†, S. S. (Bob) DAVIS† and Stephen E. HARDING*[1]

*University of Nottingham, NCMH Physical Biochemistry Laboratory, School of Biosciences, Sutton Bonington LE12 5RD, U.K., and †University of Nottingham, School of Pharmacy, University Park, Nottingham NG7 2RD, U.K.

Atomic force microscopy has been utilized to probe, at a molecular level, the interaction between purified pig gastric mucin (PGM) and a mucoadhesive cationic polymer, chitosan (sea cure 210+), with a low degree (approx. 11 %) of acetylation. Images were produced detailing the structures of both PGM and chitosan in 0.1 M acetate buffer (pH 4.5), followed by the complex of the two structures in the same buffer. PGM in 0.1 M acetate buffer revealed long linear filamentous structures, consistent with earlier electron microscopy and scanning tunnelling micoscopy studies. The chitosan molecules also adopted a linear conformation in the same buffer, although with a smaller average length and diameter. They appeared to adopt a stiff-coil conformation consistent with earlier hydrodynamic measurements. The complexes formed after mixing PGM and chitosan together revealed large aggregates. In 0.1 M ionic strength buffer they were of the order of 0.7 μm in diameter, consistent with previous electron microscopy studies. The effect of ionic strength of the buffer on the structure of the complex was also studied and, together with molecular hydrodynamic data, demonstrates that the interaction is principally electrostatic in nature.

Key words: electrostatic complex, interaction, ionic strength.

INTRODUCTION

The last two decades have seen major inroads into our understanding of the molecular architecture of the mucosal layers, which line the gasterointestinal, tracheobronchial, reproductive and ocular systems [1–5]. These advances have been paralleled with increasing efforts by the pharmaceutical industries to develop more efficient ways of delivering drugs. Many of these delivery routes, particularly those through the nasal, ocular, reproductive and gastrointestinal systems, involve contact with mucosal surfaces. The gastrointestinal route has been particularly popular among medical staff and patients alike. Although convenient, unfortunately, this route can be very inefficient for a number of reasons, including too rapid transit of the drug-containing delivery system (powder, tablet, suspension, capsule etc.) past the optimum site for absorption, which is normally the small intestine, and, to a lesser degree the stomach and colon. Resolution of this problem would be particularly important in the case of controlled-release drug delivery systems, designed to deliver drugs over extended periods of time (12–24 h). An ideal oral sustained-release dosage form should be comparable to an intravenous infusion, which continuously supplies the amount of drug needed to maintain constant plasma levels once a steady-state has been reached [6].

Attempts are being made to develop mucoadhesive polymer carrier systems for drugs that interact with the mucosal surface in a favourable way. Prime targets have been the gastrointestinal tract and also the ocular surface to (1) retard the natural clearing action of the body, slowing down the transit through the optimal sites of absorption in the stomach, intestine and colon [7] and (2) slow down the washing away action on the surface of the eye [8], respectively. In order to develop the most efficient systems, a sensible approach is to take advantage of the considerable advances in our knowledge of the structure and molecular biology of the principal macromolecular component of mucus, which largely dictates the physical properties of mucus. This is the mucus glycoprotein, or 'mucin', a large [approx. (5–50) thousand kDa] linear polypeptide decked with O-linked carbohydrate side chains, with the carbohydrate forming the bulk of the molecule (approx. 80 %).

The mucoadhesive potential of a range of polymeric substances has already been examined by molecular hydrodynamics, electron microscopy and scanning tunnelling microscopy (see [7] and references therein). One of the most promising substances appears to be derived from the insoluble polysaccharide, chitin [β-(1 → 4)-linked poly-*N*-acetylglucosamine]. The derivative is the soluble cationic polymer chitosan, formed from partial deacetylation of the chitin. Interactions with mucin appear to be both electrostatic, via NH_3^+ groups on the chitosan with either COO^- or SO_3^- groups on the mucin carbohydrate side chains, and/or hydrophobic, via $-CH_3$ groups on acetylated chitosan residues with $-CH_3$ groups on mucin side chains [depending on the degree of acetylation of the chitosan, local solvent conditions (pH, ionic strength) and the degree of sulphonation and sialic acid content of the mucin]. These molecular studies have been supported by macroscopic studies involving mechanical measurements based around the tensiometry principle on whole mucus [9].

We now seek to take advantage of the development of the powerful imaging potential of atomic force microscopy (AFM) [10] to (1) examine the structure of a gastrointestinal mucin, pig gastric mucin (PGM), (2) examine the structure of a chitosan with a low degree of acetylation (i.e. 11 %) and (3) investigate the interaction of these molecules, already established by molecular hydrodynamic, electron microscopy and scanning tunnelling microscopy probes.

AFM does not require invasive and destructive sample preparation before analysis, unlike most electron microscopic procedures [11], and facilitates the imaging of samples under ambient

Abbreviations used: AFM, atomic force microscopy; PGM, pig gastric mucin; APTES, aminopropyl-triethoxysilane; RMS, root-mean-square; SC210+, sea cure +210; *z*, vertical displacement.

[1] To whom correspondence should be addressed (e-mail Steve.Harding@nottingham.ac.uk).

temperatures and liquid environments. A recent study [12] has successfully demonstrated the virtue of this approach to the study of ocular mucins. We now focus on gastrointestinal mucin and its mucoadhesive properties with this methodology.

MATERIALS AND METHODS

Materials

PGM (sample MD [13]), was purified and isolated according to the modified procedure described in [14]. The purified mucin preparations were gently defrosted and dialysed into buffer overnight at 4 °C before use. Their molecular integrity (molecular mass distribution) was checked by size-exclusion chromatography coupled to multi-angle laser light scattering ('SEC-MALLS'), as first applied to mucins by Jumel et al. [15]. Sea cure +210 (SC210+), a glutamate salt of chitosan (Pro-Nova Ltd., Drammen, Norway), was used. This is a preparation with a degree of acetylation of 11%, which has previously been well-characterized in our laboratory [16].

Sample preparation for AFM

Freshly cleaved mica (Agar Scientific, Essex, U.K.) was silanized with aminopropyl-triethoxysilane (APTES). The mica pieces were placed into a glass Petri-dish and three drops of APTES solution were placed on the inner side of the cover. The Petri-dish was then sealed with Parafilm and the sheets were left for 2 h at room temperature. Mucin, chitosan and mixture solutions prepared in 0.1 M sodium acetate buffer, pH 4.5 containing 0.1 M NaCl, [13] were pipetted (20 μl) into an eppendorf. Glycerol solution [15–25% (v/v)] was then added to a volume of 0.5 ml and left for 30 min. The mica sheets were subsequently coated with the sample solution for 30 s, rinsed with deionized water and then dried with argon. AFM investigation was performed immediately after sample preparation.

AFM

All imaging was performed in air with a Nanoscope IIIa (Digital Instruments, Santa Barbara, CA, U.S.A.). TappingMode™ was employed with a probe constructed from silicon with a length and resonant frequency of 125 μm and 307–375 kHz, respectively (Digital Instruments, Santa Barbara, U.S.A.). All measurements made on the images of structures such as root-mean-square (RMS) 'roughness', vertical displacement (z) and size (width and diameter) were made utilizing the operating software provided with the Nanoscope IIIa AFM. Simultaneously with topographic imaging, phase data were recorded. Such data can reveal contrast based upon adhesion or viscoelastic heterogeneity in a sample surface [17].

RESULTS AND DISCUSSION

Control surfaces

In order to reveal both the thin filamentous nature of the gastric mucin structure previously shown with transmission electron

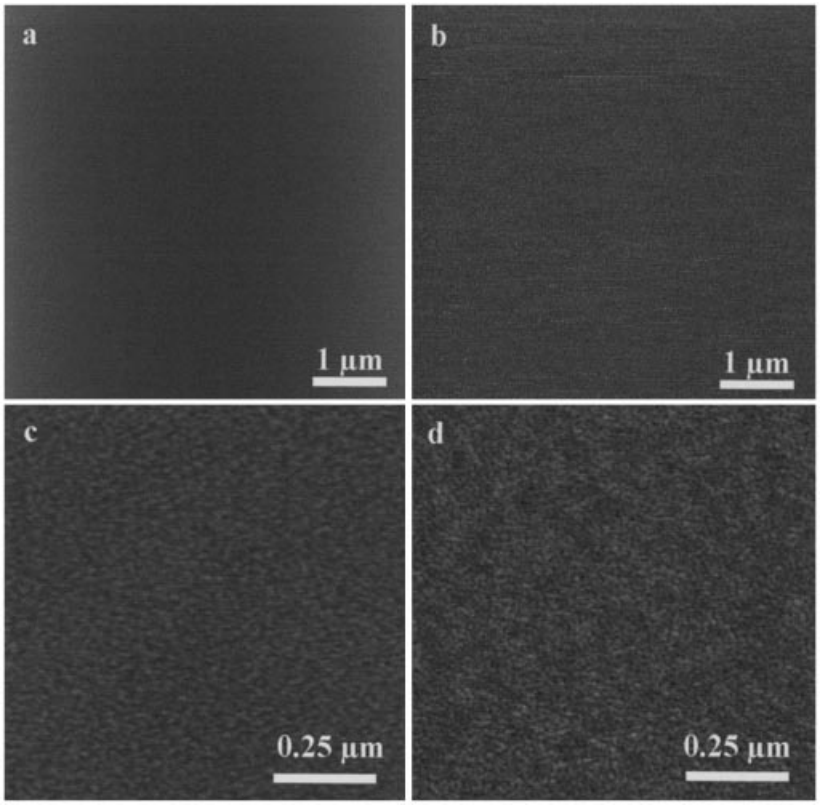

Figure 1 AFM of the substrate mica and APTES-coated mica

Mica (topography) (**a**), mica (phase) (**b**), APTES-coated mica (topography) (**c**) and APTES-coated mica (phase) (**d**).

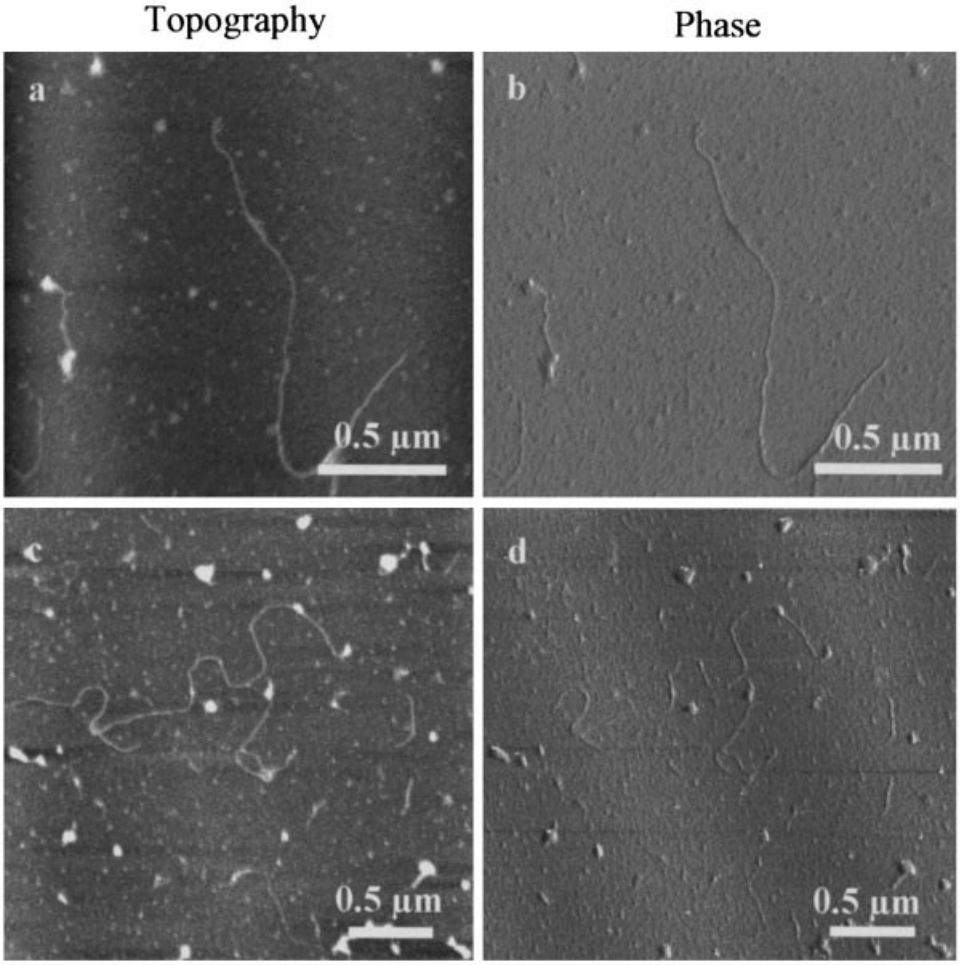

Figure 2 AFM images of purified PGM in 0.1 M ionic strength sodium acetate buffer

Topography images (**a** and **c**) and phase images (**b** and **d**).

[18–20] and scanning tunnelling microscopy [21], together with the previously unvisualized characteristics of chitosan, an extremely flat sample substrate is required. To this end, mica was chosen for this study. Figures 1(a) and 1(b) show an AFM image (topography and phase, respectively) of a clean mica surface. It is evident from this figure that the surface of this sample substrate is flat and featureless with a RMS roughness of 0.11 nm and a 'total z movement' of 0.9 nm (vertical distance moved by the z-piezoelectric scanner in AFM). Hence any further adsorbed material in future sample preparations should be apparent against such a background. Figures 1(c) and 1(d) show topography and phase AFM images, respectively, of the mica sheet that had been treated with APTES. As before, the sample substrate surface was flat and featureless with an RMS roughness of 0.14 nm and total z movement of 1.03 nm. APTES treatment was necessary to attach amino groups to the surface of the mica, to enhance the attraction of the large mucin structures. This attraction has been attributed to a charge interaction between the positive amino groups and the sialic acid or sulphate residues on the mucosal glycoproteins. Structural studies have indicated that the negative charge on PGM is thought to be attributed mostly to the amount of sulphated O-linked oligosaccharide residues in the glycosylated region and not to the amount of sialic acid present [22].

PGM glycoprotein

With the previous imaging studies on PGMs by transmission electron microscopy [18–20], to facilitate visualization it had been necessary to coat the substrate with a thin layer of conductive material, and the mucins themselves were sprayed onto the surface of this substrate. The advantage of AFM over this is that the mucins may be adsorbed directly from solution and do not require further sample treatment prior to visualization.

Figure 2 shows both topography and phase images of PGM adsorbed from solution onto the APTES-treated mica surface. The images were selected at random and are representative of a large library of images, which portray similar structural information and surface coverage. The PGM appears as long filamentous strands, which is in good agreement with previous studies using electron and scanning tunnelling microscopy [18–21], and consistent with the swollen coil array/linear random coil model for mucins [4,23]. The characteristic flattened areas along the backbone seen earlier from electron microscopy for PGM and earlier for bronchial mucins [23] were notably absent. These flattened areas were considered to correspond to the areas of high glycosylation along the polypeptide chain, the flattening

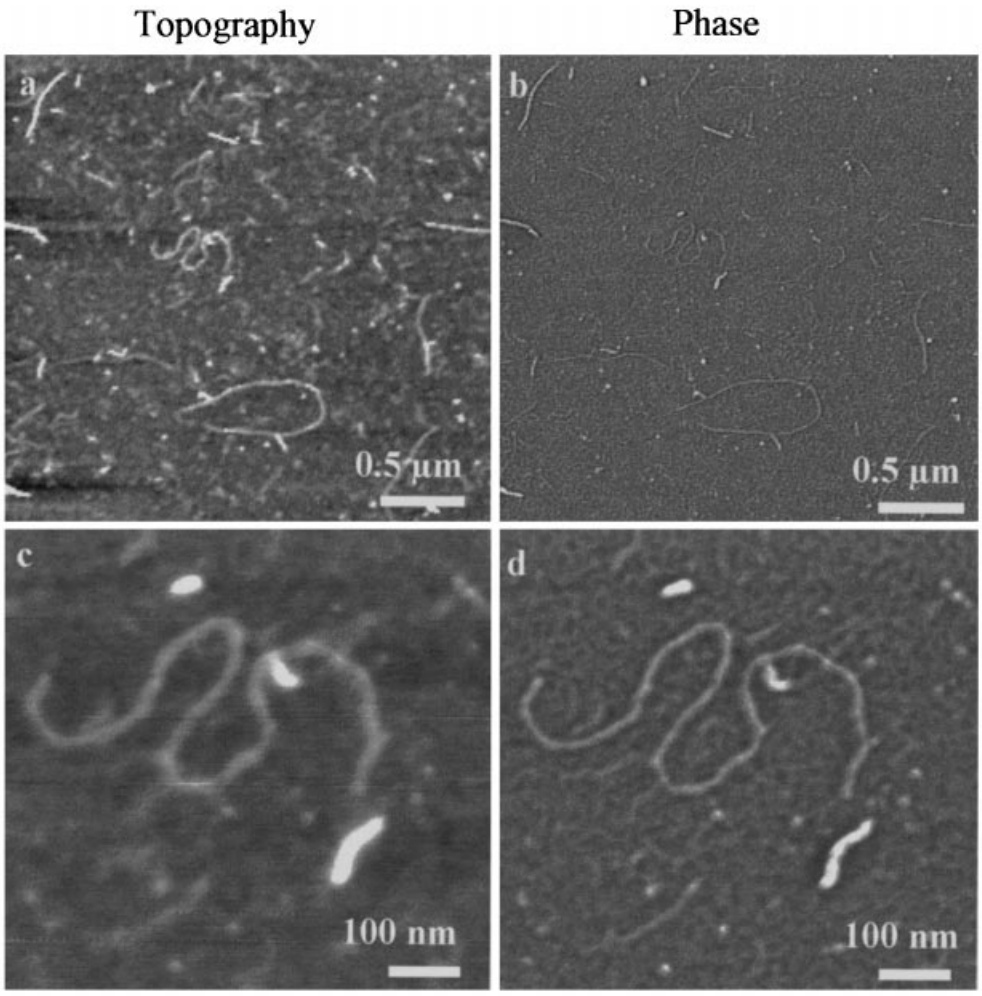

Figure 3 AFM images of chitosan SC210+ in 0.1 M ionic strength sodium acetate buffer

Topography (**a**), phase (**b**), topography (close up) (**c**) and phase (close up) (**d**).

caused by the effect of the vacuation on areas of very high hydration [23]. The molecule would not have been subject to these effects for AFM visualization, and therefore it is not surprising that these regions were not evident from AFM.

From the AFM images of Figure 2 and similar, the average length of the PGM molecules was determined to be approximately $2.00 \pm 0.55\ \mu$m, which agrees with studies performed with transmission electron microscopy and sedimentation equilibrium experiments [3,4]. However, occasionally some PGM filaments were seen to possess a maximum length of nearly $4\ \mu$m and a minimum of $0.5\ \mu$m, reflecting the polydisperse nature of the material. The diameters of the filaments were approximately constant, at 16 nm.

Chitosan SC210+

Figure 3 illustrates AFM images of the chitosan (SC210+) molecules. It is possible to see from the larger $0.5\ \mu$m image (Figures 3a and 3b) that the structure is extremely polydisperse, with the polysaccharide chain lengths varying extensively. The average length of the polysaccharide was approx. $0.70 \pm 0.27\ \mu$m, which is smaller than the average backbone length for the PGM. The widths of these polymer chains were very consistent, being approx. 11 nm, which is smaller than for the PGM. This is consistent with the absence of side chain branches in the chitin/chitosan structure. Figures 3(c) and 3(d), which appear to represent a single chitosan chain, reveal that there are no obvious structural features to distinguish this from the mucin glycoprotein. However, the molecules appear to adopt a stiff-coil conformation, consistent with these molecules being Zone B (rigid rod) or Zone C (semi-flexible coil) structures [24,25] depending on the chain length, the shorter chains being more rigid.

Immobilization strategy

The immobilization strategy chosen for this study was aimed at immobilizing the much larger of the two molecules, namely the mucin. A positive surface potential was created to attract the somewhat negatively-charged mucin glycoproteins. Naturally one would not expect any charge attraction between the positively-charged chitosan molecule and the positively-charged surface. However, such observations have been made in the extensive studies of DNA by AFM, whereby negatively-charged DNA is immobilized onto negatively-charged bare mica using $MgCl_2$ or similar buffers [26,27]. The Mg^{2+} ions shield the repulsion that would otherwise occur between the DNA and the mica. Interestingly it has been noted by Bezanilla et al. [26] that

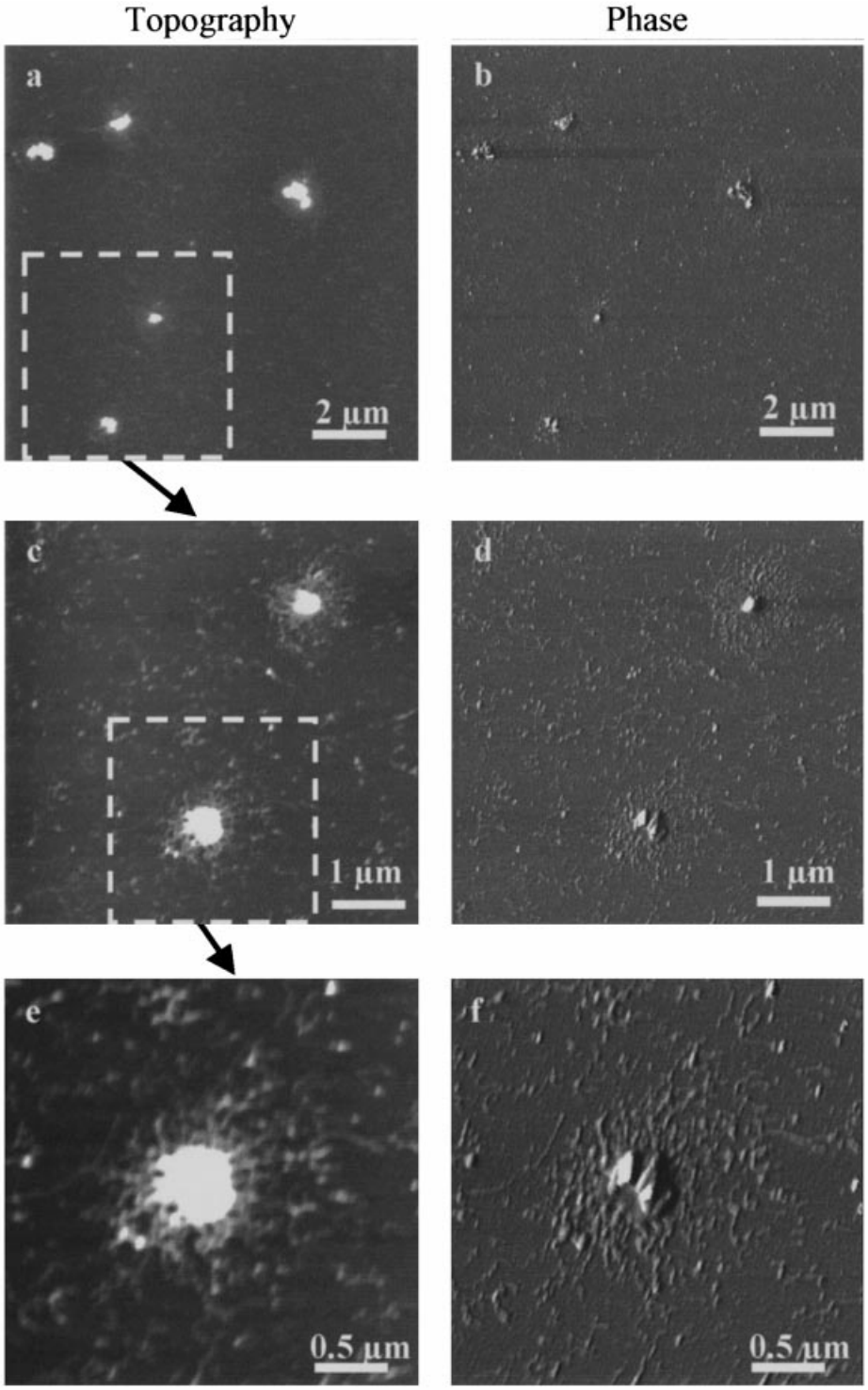

Figure 4 AFM images of PGM complexed with chitosan SC210+ in 0.1 M ionic strength sodium acetate buffer at different degrees of magnification

Figures (**a**, **c** and **e**) were recorded using the topography mode. Figures (**b**, **d** and **f**) were obtained in the phase mode, giving much crisper images.

a lack of DNA adhesion occurs as ionic strength increases, suggesting that the DNA prefers to remain in solution as the ionic strength increases. In a similar fashion we also observed a lack of chitosan adhesion when using higher ionic strength solutions (results not shown).

It is also worth noting that at the lower ionic concentrations employed (0.1 M) the counterion concentration appears insufficient to suppress the repulsive forces between the positively-charged deacetylated units situated along the polymer backbone, which keep the polymer in the extended linear arrangement

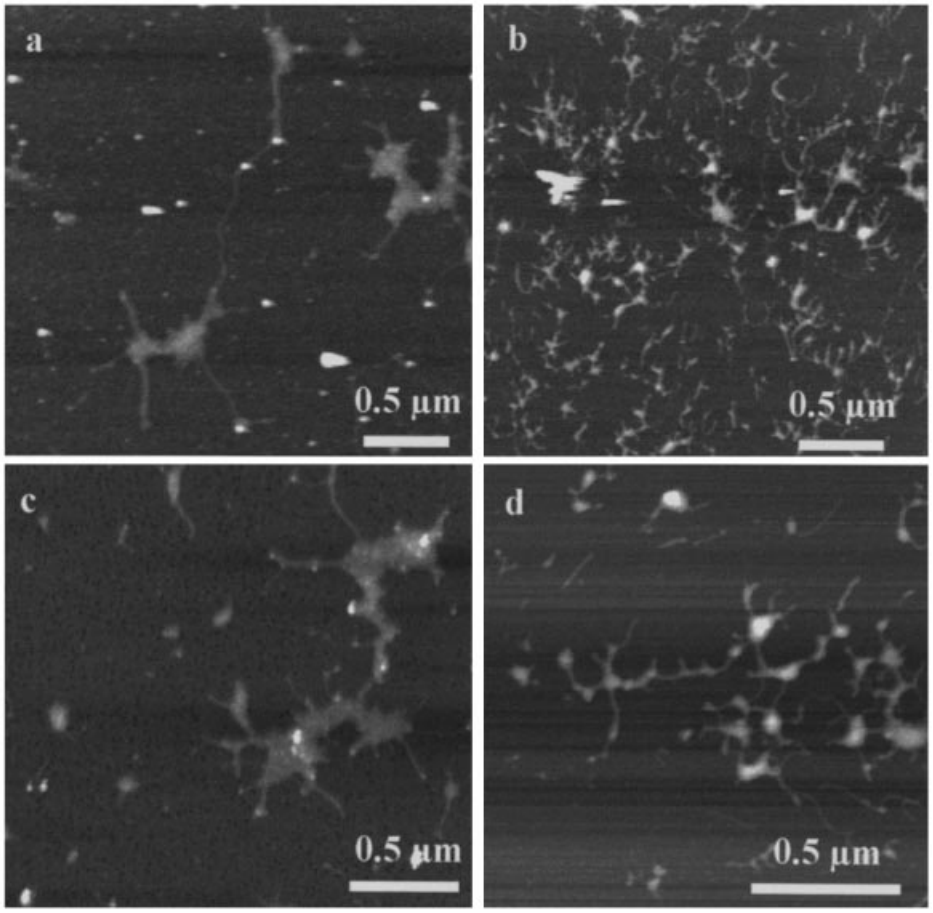

Figure 5 AFM topography images of PGM and PGM complexed with chitosan SC210+ in 0.2 M and 0.3 M ionic strength sodium acetate buffer

PGM at 0.2 M (**a**), PGM–SC210+ complex at 0.2 M (**b**), PGM at 0.3 M (**c**) and PGM–SC210+ complex at 0.3 M (**d**).

observed. As the ionic concentration is increased this repulsion effect is reduced resulting in a more coiled arrangement of the polymer [28]. This may also contribute to the lack of chitosan visualized on the surface at the elevated ionic concentrations.

Complexes of PGM and chitosan at 0.1 M ionic strength

As has been previously indicated [7,19,20,29] a significant interaction has been shown between the purified PGM and this form of chitosan on the basis of molecular hydrodynamics, electron microscopy and scanning tunnelling microscopy, consistent with macroscopic tensiometry studies [9]. Figure 4 illustrates the complex formed between the chitosan and mucin structures when mixed together in solution and then immobilized to the APTES-coated substrate. Instead of the characteristic filamentous nature of both the chitosan and PGM (Figures 2 and 3, respectively) large clump-like aggregates were observed, consistent with the electron microscopy observations of Fiebrig et al. [19,20]. The average diameter of these aggregates, determined by taking two diameter measurements (x and y) on a large number of aggregates (20) was approx. 0.70 ± 0.18 μm (some complexes were seen with radial diameters of approx. 0.3 μm and some as large as approx. 1.2 μm). Surrounding these aggregates was a tangled arrangement of filaments that seemed to emanate from the central aggregate. The diameter of these filaments was approx. 16 nm. This suggests that these filaments were strands of PGM radiating from the complex.

Complexes of PGM and chitosan at 0.2 M and 0.3 M ionic strength

Earlier hydrodynamic studies [13,29] have shown a clear effect on mucin–chitosan complexes by increasing the ionic strength. Figure 5 shows the characteristic mucin (Figures 5a and 5c) and complex (Figures 5b and 5d) structures at 0.2 M and 0.3 M ionic strength, respectively. It is apparent that the structure of the mucin at 0.2 M and 0.3 M ionic strength is quite different to that at 0.1 M ionic strength. At 0.2 M (Figure 5a) the long filamentous structure seen at 0.1 M is no longer present. It was difficult to measure the average length of the mucins at this molar concentration as the structures seemed to be formed from a number of mucin filaments. However, where an individual filament was evident, the average width was equivalent to that in the 0.1 M solution, i.e. approx. 16 nm. This apparent mucin self-interaction effect became more pronounced at the higher 0.3 M ionic strength, shown in Figure 5(c). At this ionic strength there seemed to be many filaments interacting to form more complex aggregates of mucin. The only mucins available for analysis of dimensions were those which emanated from the complex. The average diameter was again 16 nm, but the average length was impossible to determine due to the extent of interaction. If the number of mucin strands which emanate from the mucin complex are counted it shows that, on average, over many complexes imaged, at 0.2 M there are 3–4 mucin strands and at 0.3 M there are 10–11 mucin strands interacting to form the complex. Clearly,

increasing the ionic strength seems to promote self-association among the mucin molecules. Ionic strengths < approx. 0.2 M (including physiological conditions) appear to be insufficient to suppress charge repulsion effects on the charged mucin side chains, hence the mucins remain unassociated.

The images presented in Figures 5(b) and 5(d) are the structures of the complexes from the mucin/chitosan mixtures at 0.2 M and 0.3 M ionic strength, respectively. These also display some differences from the structures observed at 0.1 M (Figure 4). While there still appears to be some degree of complex formation between the mucin and chitosan, the size of the complexes is greatly reduced. At 0.1 M large aggregates formed that had an average diameter of 0.7 μm, while at 0.2 M and 0.3 M the smaller aggregate structures visualized had an average diameter of approx. 150 nm (visualized in the same way as those structures at 0.1 M). Noticeably there is a greater number of these 'muco-adhesive complexes' at 0.1 M ionic strength, suggesting a reduction in interaction between the mucin and chitosan as the ionic strength increases beyond physiologically relevant conditions, and consistent with what was observed earlier by molecular hydrodynamics [7,29]. Charge suppression clearly reduces the amount of electrostatic interaction. Although the higher ionic strengths do not represent physiological conditions, the experiments across the range of ionic strengths do appear to demonstrate that it is indeed electrostatic interactions that are important for (1) keeping mucins apart through inter-chain repulsion and (2) promoting mucoadhesive interaction at low (physiological) ionic strength conditions.

Conclusions

There now exists irrefutable evidence that chitosans interact with mucins. The findings in the present study, based on AFM imaging, clearly support the earlier molecular data based on molecular hydrodynamics, electron microscopy and scanning tunnelling microscopy [7]. Molecular imaging, which 'visualizes' macromolecules, coupled with molecular hydrodynamics, which refers to macromolecules in their 'natural physiological state' unperturbed by sample preparation protocols, is clearly a powerful combination for the study of this and other heterogeneous molecular systems. The main contribution towards the interaction is clearly electrostatic, with some hydrophobic contribution [7]. The AFM data also support the macroscopic tensiometric measurements [9]. This demonstration should assist with the design of more efficient gastrointestinal drug delivery systems [30,31].

M. P. D. was in receipt of a BBSRC CASE studentship with Optokem Ltd. (Mold, U.K.).

Received 2 December 1999/18 February 2000; accepted 27 March 2000

REFERENCES

1 Allen, A., Pain, R. H. and Robson, T. H. (1976) Nature **264**, 88–89
2 Creeth, J. M. (1977) Mod. Probl. Paediatr. **19**, 34–35
3 Harding, S. E. (1989) Adv. Carbohydr. Chem. Biochem. **47**, 345–381
4 Sheehan, J. K. and Carlstedt, I. (1989) in Dynamic Properties of Biomolecular Assemblies (Harding, S. E. and Rowe, A. J., eds.), pp. 256–275, Royal Society of Chemistry, Cambridge, U.K.
5 Gum, J. R. (1995) Biochem. Soc. Trans. **23**, 795–799
6 Forster, H. and Lippold, B. C. (1982) Pharmaceutica Acta Helvetica **57**, 345–349
7 Harding, S. E., Davis, S. S., Deacon, M. P. and Fiebrig, I. (1999) Biotechnol. Gen. Eng. Rev. **16**, 41–86
8 Greaves, J. L. and Wilson, C. G. (1993) Adv. Drug Delivery Rev. **11**, 349–383
9 Lehr, C.-M., Bouwstra, J. A., Schacht, E. H. and Junginger, H. E. (1992) Int. J. Pharm. **78**, 43–48
10 Binnig, G., Quate, C. F. and Gerber, C. H. (1986) Phys. Rev. Lett. **56**, 930–933
11 Kirby, A. R., Gunning, A. P. and Morris, V. J. (1995) Trends Food Sci. Technol. **6**, 359–365
12 McMaster, T. J., Berry, M., Corfield, A. P. and Miles, M. J. (1999) Biophys. J. **77**, 533–541
13 Deacon, M. P., Davis, S. S., White, R. J., Nordman, H., Carlstedt, I., Errington, N., Rowe, A. J. and Harding, S. E. (1999) Carbohydr. Polym. **38**, 235–238
14 Hutton, D. A., Pearson, J. P., Allen, A. and Foster, S. N. E. (1990) Clin. Sci. **78**, 265–271
15 Jumel, K., Fiebrig, I. and Harding, S. E. (1996) Int. J. Biol. Macromol. **18**, 133–134
16 Errington, N., Harding, S. E., Vårum, K. M. and Illum, L. (1993) Int. J. Biol. Macromol. **15**, 113–117
17 Chen, X., Daview, M. C., Roberts, C. J., Tendler, S. J. B., Williams, P. M., Davies, J., Dawkes, A. C. and Edwards, J. C. (1998) Ultramicroscopy **75**, 171–181
18 Sheehan, J. K., Oates, K. and Carlstedt, I. (1986) Biochem J. **239**, 147–153
19 Fiebrig, I., Harding, S. E., Rowe, A. J., Hyman, S. C. and Davis, S. S. (1995) Carbohydr. Polym. **28**, 239–244
20 Fiebrig, I., Vårum, K. M., Harding, S. E., Davis, S. S. and Stokke, B. T. (1997) Carbohydr. Polym. **33**, 91–99
21 Roberts, C. J., Shivji, A., Davies, M. C., Davis, S. S., Fiebrig, I., Harding, S. E., Tendler, S. J. B. and Williams, P. M. (1995) Protein Pept. Lett. **2**, 409–414
22 Nordman, H., Davies, J. R., Herrman, A., Karlsson, N. G., Hansson, G. C. and Carlstedt, I. (1997) Biochem. J. **326**, 903–910
23 Harding, S. E., Rowe, A. J. and Creeth, J. M. (1983) Biochem. J. **209**, 893–896
24 Pavlov, G. M., Rowe, A. J. and Harding, S. E. (1997) Trends Anal. Chem. **16**, 401–405
25 Tombs, M. P. and Harding, S. E. (1998) in An Introduction to Polysaccharide Biotechnology, pp. 144–147, Taylor & Francis, London.
26 Bezanilla, M., Bustamante, C. J. and Hansma, H. G. (1993) Scanning Microsc. **7**, 1145–1148
27 Rabke, C. E., Wenzler, L. A. and Bebbe, Jr., T. P. (1994) Scanning Microsc. **8**, 471–480
28 Skaugrud, O., Hagen, A., Borgesen, B. and Dornishm, M. (1999) Biotechnol. Gen. Eng. Rev. **16**, 23–40
29 Fiebrig, I., Harding, S. E. and Davis, S. S. (1994) Prog. Colloid Polym. Sci. **93**, 66–73
30 Fiebrig, I., Harding, S. E. and Davis, S. S. (1995) in Biopolymer Mixtures (Harding, S. E., Hill, S. E. and Mitchell, J. R., eds.), pp. 373–419, Nottingham University Press, Nottingham
31 Mathiowitz, E., Chickering, III, D. E. and Lehr, C.-M. (1999) Bioadhesive Drug Delivery Systems. Fundamentals, Novel Approaches and Development, Marcel Dekker, New York